Morphogen signalling patterns calcium waves in the *Drosophila* wing disc

Qinfeng Wu[1,*], Pavel Brodskiy[1,*], Cody Narciso[1], Megan Levis[1], Ninfamaria Arredondo-Walsh[1], and Jeremiah J. Zartman[1,#]

[1]Department of Chemical and Biomolecular Engineering, University of Notre Dame, 205D McCourtney Hall, Notre Dame, IN 46556, USA

*These authors contributed equally to this work

[#]Email for correspondence: jzartman@nd.edu

Key words:

Quantitative biology; pattern formation; signal transduction; dynamic systems; reverse engineering; developmental biology; image analysis

Abstract

Intercellular Ca^{2+} waves (ICWs) are multicellular, coordinated oscillations of Ca^{2+} that transverse tissues and are functionally implicated in development, regeneration, and diseases such as cancer. However, the extent that spontaneous ICWs are a regulated phenomenon controlled by cell-cell communication networks is unclear. Here we report that ICWs exhibit spatiotemporal patterns at the organ-level using a new image analysis algorithm to quantify ICW dynamics. ICWs in the *Drosophila* wing disc require a specific phospholipase C, Plc21C. Further, we demonstrate that the morphogen signalling pathway, Hedgehog, modulates ICW frequency uniformly in the tissue through two distinct routes and is required for non-uniform spatial patterning of ICW amplitudes. Thus, the dynamics of spontaneous ICWs are regulated by morphogenetic signalling through two orthogonal mechanisms—frequency and amplitude—and provide an organ-scale communication system for the developing wing disc.

Introduction

Calcium (Ca^{2+}) is a ubiquitous second messenger that is a central player in cellular differentiation, proliferation, wound healing and regeneration[1–7]. Ca^{2+} signals are usually oscillatory and can encode information through several features, including peak amplitudes, frequencies, normalized wave widths measured by duty cycle, and basal cytoplasmic concentrations[8–10]. Spontaneous intercellular Ca^{2+} waves (ICWs) occur in many tissue types. For example, ICWs are involved in ensuring robust wound healing and regeneration[4,6,11] and have been observed in multicellular developmental contexts such as butterfly pupal wings[12] and in *Drosophila* larval wing discs[6]. However, whether and how ICWs are spatiotemporally regulated at the organ scale is largely unknown. Understanding the regulation of ICWs in organs will provide insights into development[13–15], as well as diseases such as Alzheimer's disease[16] and metastatic cancers[17].

Organ development relies on precise, long-range communication of information among cells. During development, spatial information is conveyed by the concentration of morphogens that specify cell fates[18]. For example, Hedgehog (Hh) is an important morphogen that directs anterior-posterior (A/P) cell identity in tissues of most animals with bilateral symmetry[19]. Hh signalling is also essential for specifying the A/P patterning in the *Drosophila* wing disc, which develops into the wing of the adult fly and has led to many discoveries defining mechanisms of organ development[19–21]. Hh signalling has two mechanistic branches: 1) slower, canonical signalling, through regulation of the transcription factor *cubitus interruptus (ci)*, and 2) fast, noncanonical signalling, through the protein $G\alpha_i$ [22]. A recent study has shown that noncanonical Hh signalling regulates Ca^{2+} in frog neural tubes[23], but the spatiotemporal regulation of Ca^{2+} signalling by Hh and other morphogens is unknown.

Results

Fly serum based extracts stimulate ICWs *ex vivo*

To study ICWs in wing discs, we used the GCaMP6f sensor to visualize relative concentrations of cytoplasmic Ca^{2+} in the wing disc pouch (Fig. 1a)[24]. We experimented with two different imaging methods. We first imaged *Drosophila* larvae using an *in vivo* imaging setup to characterize ICW activity in the wing disc pouch (Fig. 1b)[6]. We observed spontaneous ICWs in 35% of larva imaged over a twenty-minute period (n = 25/72), in qualitative agreement with a recent study[6] (Fig. 1d, d', Extended Data Movie 1). However, *in vivo* imaging provides limited information due to larval motion, mechanical compression, and an inability to specifically perturb the organ with drugs[25–27].

Therefore, we cultured discs *ex vivo* to enable higher resolution imaging (Fig. 1c). We initially used the chemically-defined ZB media, which supports culture of wing disc-derived Clone 8 cells for over 100 passages as a starting point to identify possible chemical signals impacting ICW activity[28]. Discs cultured in ZB media without fly extract did not yield ICWs (Fig. 1e, e', Extended Data Movie 2). We found that supplementation of ZB media with fly extract (FEX)[28], which is serum produced from ground flies, led to ICWs in wing discs (Fig. 1f, f', Extended Data Movie 3). Therefore, FEX is necessary and sufficient to produce ICWs.

ICWs require specific components of the Ca^{2+} signalling pathway

To quantify ICW dynamics, we developed an image analysis algorithm to extract Ca^{2+} signatures from each disc (Fig. 2a, Extended Data Fig. 1-3), and combine them into multi-disc composites (Fig. 2b, c, Extended Data Fig. 1-3). The algorithm calculates the relative amplitudes, which represent the average magnitude of these events; frequencies, which represent the numbers of events over time; duty cycle, which represents the fraction of time that a cell is active; and basal intensity levels, which reflect the basal Ca^{2+} concentration of a cell not undergoing a spike (Fig. 2b). Composites were generated showing the average spatial distribution of these summary statistics within the pouch and between samples (Fig. 2c, Extended Data Fig. 1-3).

To elucidate the mechanism behind FEX-induced ICWs, we used RNA interference (RNAi) to systematically knock down components of the Ca^{2+} signalling pathway (Fig. 2d) and measured changes in ICW dynamics. Phospholipase C (PLC) catalyses the production of inositol-1,4,5-triphosphate (IP_3), which binds to and stimulates IP_3 receptor (IP_3R) on the endoplasmic reticulum (ER) to release Ca^{2+} from the ER (Fig. 2d). However, the isoform of PLC responsible for stimulating ICWs is unknown. We tested all PLC homologs in *Drosophila* for a Ca^{2+} wave phenotype. We found that expression of *Plc21C*^{RNAi} (PLCβ1 homolog), completely extinguishes ICW activity in the wing disc (Fig 2d, Extended Data Movie 4). Knockdown of the other PLC homologs—PLCγ homolog *small wings* (*sl*) and PLCβ4 homolog *norpA*—did not affect ICWs (Fig. 2e, Extended Data Movie 5, 6). Additionally, we confirmed several of the components previously implicated in Ca^{2+} signalling in the wing disc are required for ICW dynamics through RNAi experiments: ICWs require Ca^{2+} release through IP_3R, Ca^{2+} recycle through SERCA and diffusion through gap junctions[6,11,28,29] (Extended Data Movie 7-9). Ca^{2+} channels Stim, Orai and PMCA did not qualitatively impact the presences of ICWs (Extended Data Movie 10-12).

Spatial patterning of ICW signatures emerges throughout development

We noted a striking difference in Ca^{2+} intensity between the anterior (A) and posterior (P) compartments of wing discs (Fig.1a, 2), suggesting spatial patterning of Ca^{2+} signals. For all discs imaged, 72% of discs had higher average amplitudes (Amp) in the P compartment (2-tailed Student's t-test, $p<3x10^{-4}$, n=87). The average Amp is 30% higher in the P compartment than the A compartment (Fig 3a, Extended Data Table 1). To further investigate spatiotemporal patterning of Ca^{2+} signatures, we examined spatial distributions of Ca^{2+} signatures in pouches of different developmental ages. To do so, we grouped the wing discs by pouch size, which can be used to approximate the developmental age of a larva[30] (Fig. 3, Extended Data Table 1). We found that the difference in amplitudes between compartments increases with increasing pouch size (Fig. 3a, b, Extended Data Table 1). The duty cycle is not correlated with pouch size, and was not spatially patterned between compartments in the pouch (Fig. 3a, d). Basal intensity decreases with increasing pouch size (ANOVA, $p<4x10^{-4}$, Fig. 3a, e). Averaged over the compartment level, frequencies are not significantly different ($p>0.05$), which likely indicates that frequency is driven primarily by diffusion, while the driving force behind amplitude is the difference between Ca^{2+} concentration in the cytoplasm and ER of individual cells (Fig. 3a, c). These results show that that the overall basal level decreases as the discs mature and that a

spatial patterning of ICW amplitudes across the A-P axis emerges at later stages of development. The spatial patterning of ICW activity during wing disc growth suggests that ICWs can convey long-distance spatial information to cells, in effect providing a memory of morphogenetic spatial information[31].

Canonical Hh signalling modulates ICW frequency and directs amplitude patterning

The discovery of A/P patterning of average ICW amplitudes led us to suspect the involvement of Hh signalling, which directs the development of the A and P compartment boundary[32–34] (summarized in Fig. 4a) and plays roles in wing disc regeneration[35]. Hh signalling activity is dependent on the protein Smoothened (Smo), whose activity is inhibited by the receptor Patched (Ptc)[21]. Smo binds to the Hedgehog Signalling Complex (HSC) containing the protein Costal2 (Cos2), the kinase Fused (Fu) and the transcriptional factor Cubitus interruptus (Ci)[21]. In the absence of Hh, HSC controls the cleavage of full length Ci (Ci155) to a truncated repressor form, Ci^{R}[21]. Suppressor of Fused (SuFu) retain Ci155 in the cytoplasm to oppose its nuclear import[36]. Binding of Hh to Ptc blocks Ptc-mediated Smo inhibition, allowing Smo to signal to reduce Ci cleavage[21]. Noncanonical Hh signalling is the result of the activation of $G\alpha_i$ by Smo[22]. $G\alpha_i$ has many downstream effects including reducing the concentration of cyclic AMP (cAMP), which in turn inhibits Protein Kinase A (PKA)[22].

To determine the effect of canonical Hh signalling on ICWs, we analysed ICWs in genetically perturbed wings. The knockdowns were validated by examination of the wing phenotypes (Extended Data Fig. 4, Extended Data Table 2). Canonical Hh activators tended to have lower average frequencies in the pouch than the control (control: 0.76 ± 0.21 mHz, UAS-*ci*: 0.51 ± 0.22 mHz, $p<0.02$, and UAS-ci^{PKA-}: 0.93 ± 0.39 mHz, $p<0.002$, Fig. 4b-e, Extended Data Movie 13-15, Extended Data Table 3), and all three canonical Hh suppressors tended to have higher average frequencies than the control (smo^{RNAi}: 0.86 ± 0.17 mHz, $p<2x10^{-7}$, UAS-*cos2*: 0.96 ± 0.36, $p<0.09$, and ci^{RNAi}, 1.0 ± 0.2 mHz, $p<2x10^{-4}$ Fig. 4b-e, Extended Data Movie 16-18, Extended Data Table 3). Suppression of Smo increased average Ca^{2+} oscillation frequencies *in vivo*, where ICWs occurred twice as frequently in the smo^{RNAi} condition relative to the tester line (Fig. 4f, Extended Data Movie 19). These results demonstrate that Smo reduces ICW frequencies by a canonical mechanism. However, activation of Smo through smo^{CA} led to a multimodal distribution of average ICW frequencies in the pouch, including normal, higher ICW frequency, or severe reduction of ICWs (Extended Data Movie 20). The heterogeneous smo^{CA} data is consistent with an interpretation that smo^{CA} also activates ICWs through both canonical and noncanonical mechanisms.

To investigate the possibility of noncanonical activation of ICW frequency, we used a variety of drugs to acutely perturb the noncanonical Hh pathway and the downstream PKA pathway. Vismodegib (GDC-0449) and cyclopamine serve as antagonists to canonical Hh signalling, but agonists to Smo-based noncanonical signalling[37], which is the only signalling mechanism active on the timescale of the experiment (<2 h of incubation and imaging)[38]. SQ 22536 suppresses cAMP, a downstream target of noncanonical Hh signalling, through adenylyl cyclase inhibition. All three drugs tended to increase the ICW frequency relative to a 0.1% DMSO control (DMSO: 0.48 +/- 0.3 mHz, Vismodegib: 0.96 ± 0.26 mHz, $p<0.2$, Cyclopamine: 0.79 ± 0.13 mHz, $p<0.02$, SQ 22536: 0.85 ± 0.17 mHz, $p<7x10^{-3}$, Fig. 4b-e, Extended Data Movie 21-24, Extended Data Table 3). Together with the canonical results, this indicates that modulation of ICW frequencies by Hh follows a paradoxical signalling motif[39,40], wherein Hh signalling activity leads to reduced ICW frequency through canonical signalling and increased ICW frequency through noncanonical signalling (Fig. 4g, h).

Finally, to determine whether Hh signalling is responsible for spatial patterning of ICW amplitudes, we examined the spatial pattern of average Amp in the A and P compartments for all previously mentioned conditions (Fig. 4c). We found that in all cases, genetic perturbations (both positive and negative) of canonical Hh signalling were sufficient to abolish spatial patterning of ICW amplitudes between the A and P compartments (Fig. 4c, d). However, acute drug perturbations did not tend to alter the spatial pattern of ICW amplitudes (Fig. 4c, all $p<0.05$). One possible explanation is that the observed responses are due to the short-term effect of the drug perturbation and the short assay duration whereas genetic perturbations are inherently long-term effects with the canonical transcriptional output of Hh signalling determining the differences in average Amp responses along the A-P axis of the disc. In the experiments, discs were incubated with drugs for one hour to impact cellular processes before imaging, while the genetic perturbation is turned on at the onset of transgene expression with the *nubbin-Gal4* driver (active throughout the 3rd instar of development). Overall, these results indicate that Hh is required for amplitude patterning of ICWs through a mechanism that requires canonical signalling, which is not affected by acute drug perturbations. In this study, we did not explore long-term drug experiments out of a concern of possible artefacts that might arise from long-term *ex vivo* incubations.

Discussion

Here, we report the discovery that spontaneous ICW activity during wing disc development is regulated in part by morphogenetic signalling. Quantitative analysis reveals A/P patterning of average ICW amplitudes and temporally decreasing basal intensity as wing discs reach their terminal size before pupariation. We have also demonstrated that Hh signalling is necessary for spatial patterning of ICW amplitude, and that Hh signalling paradoxically modulates ICW frequency, through canonical reduction and noncanonical increases of frequency.

Since the stimulation of ICWs in *ex vivo* culture depends on FEX, it will be important to elucidate the active components in FEX that stimulate ICWs. Our result indicates that ICWs specifically and selectively require Plc21C (PLCβ1), and inhibition of either *sl* or *norpA* has no effect on ICW activity. Therefore, Plc21C can be used to selectively modulate ICWs in future studies. The A/P patterning of ICW amplitudes suggests a potential biological function of ICWs in conveying or storing spatial information in wing discs. One possible mechanism to be tested in the future is that Hh signalling regulates ICWs through Plc21C activity, which may be a direct regulatory target of Ci, as the *Plc21C* enhancer has Ci binding sites, and is responsive to Hh signalling[41]. Further, canonical Hh signalling has many target genes, including the Decapentaplegic and Wingless pathways. We are currently investigating the interplay between Ca^{2+} and other morphogen pathways. Hh's downstream morphogenetic signalling targets may mediate the regulation of ICW dynamics.

Our result demonstrates that Hh signalling modulates ICW frequency through an incoherent feed-forward loop (I-FFL, Fig. 4h)[42]. An I-FFL is a feed-forward loop with two arms of opposite function. I-FFLs characteristically function as pulse-generators and response accelerators[42–44]. This suggests that Ca^{2+} frequency responds to changes in Hh signalling rapidly. Additionally, chronic suppression of both legs of the I-FFL thought Smo^{RNAi} expression resulted in an increase in frequency (Fig. 4), suggesting that canonical Hh suppression has a greater effect on the steady-state frequency than noncanonical Hh activation. Uncovering the role of Ca^{2+} as an integrator of morphogenetic signalling integration in the wing disc will yield insights into the function of similar roles of crosstalk between morphogen and Ca^{2+} signalling pathways in other systems. Intriguingly, the spatial patterning of ICW amplitudes hints at an additional layer of positional information during wing disc development that may more generally be related to patterning of cell metabolism. Combined with evidence that ICWs and gap junction

communication facilitate wound healing[6,45], this evidence demonstrates that ICWs may be form a component of the posited 'memory' system required for pattern repair during tissue regeneration[31].

Acknowledgements

The work in this manuscript was supported in part by NSF Award CBET-1403887 and CBET-1553826, ND Advanced Diagnostics and Therapeutics and Harper Cancer Research Institute Research like a Champion awards (QW), Walther Cancer Foundation Interdisciplinary Interface Training Project (PB), and the Notre Dame Advanced Diagnostics & Therapeutics Berry Fellowship (CN). The authors gratefully acknowledge the Notre Dame Integrated Imaging Facility. We would like to thank Christopher Paolucci, Jeffrey Kantor, Danny Chen, Jianxu Chen, Gregory Reeves, Alyssa Lesko, Jamison Jangula and Yogesh Goyal for helpful feedback, and Brandon Greenawalt (Notre Dame Center for Social Research) for helpful conversations regarding statistical methodology, S. Restrepo for sharing unpublished observations, Jahmel Jordon for technical support as well as members of the Zartman Lab.

Author contributions

J.J.Z., Q.W. P.B. and C.N. designed and conceived the study. Q.W. and C.N. performed *ex vivo* imaging. M.L. performed *in* vivo imaging. N.A.W. performed wing imaging. P.B. developed image processing pipeline. Q.W., P.B., and J.J.Z. analysed data and wrote the manuscript. J.J.Z supervised all aspects of the study.

Methods

Fly strains and genetics

Gene perturbations to the core Ca^{2+} and Hedgehog signalling pathways (UAS-*Gene X*^{RNAi} or UAS-*Gene X* (overexpression) were crossed to a genetic tester line (*nub-GAL4*, *UAS-GCaMP6f*/*CyO*) that enables combined visualization of Ca^{2+} signalling with down regulation of genes through expression of RNAi in the wing disc. Multiple independent RNAi lines were tested for each gene investigated (Extended Data Table 2,4). Stocks are obtained from Bloomington *Drosophila* Stock Center as indicated by stock number (BL#). Progeny wing phenotypes are from F1 male progeny emerging from the nub-Gal4, UAS-GCaMP6f/CyO x UAS-X cross and shown in Fig. S5. The tester line (w1118; nubbin-GAL4, UAS-GCaMP6f/CyO) was generated by recombining P{UAS-Dcr-2.D}1, w1118; P{GawB}nubbin-AC-62 (BL#25754) with w1118; P{20XUAS-IVS-GCaMP6f}attP40 (BL#42747).

In vivo imaging setup

Wandering 3rd instar *nub-GAL4*, *UAS-GCaMP6f*/*CyO* larvae were collected for imaging and rinsed vigorously in deionized water. They were dried completely and then adhered to a coverslip for imaging with scotch tape covering the larvae. The larvae were attached with their spiracles facing toward the coverslip to insure the wing discs were aligned toward the microscope. An EVOS Auto microscope was used to image the larvae. The larvae were imaged at 20x magnification for 20 minutes; images were taken every 15 seconds.

Organ culture media

ZB media + 15% FEX contains 79.4% (v/v) ZB media, 0.6% insulin, 15% ZB-based fly extract and 5% penicillin/streptomycin[25]. ZB media was developed as a chemically defined media to support *Drosophila* cell culture[26], and was used as the basal media for most experiments. ZB-based fly extract (FEX) is undefined serum extracted from ground flies using ZB media as the base. It is commonly used in culture media as a substitute of fetal bovine serum (FBS) to support *Drosophila* tissue growth and prolong the culture time of cultured wing discs. ZB-based

FEX is made from the following protocol: One gram well-nourished mature flies, were homogenized in a tissue homogenizer (15 ml capacity, 0-1 mm clearance) with 6.82*x* ml of ZB media. This homogenate was centrifuged at 2600 rpm for 20 min at 4°C. The supernatant and the oily film above it were removed and heat-treated at 60°C for 20 min. This preparation was then spun at 2600 rpm for 90 min at 4°C. The supernatant (fly extract) was removed, sterilized by 0.2 µm filters, and stored at 4°C.

Wing disc imaging setup

Wing discs were dissected from 3rd instar larvae and cultured and imaged in the organ culture media on a cover slip based on our previously developed protocol[25]. A cell culture insert (EDM Millipore), after truncated the legs, was put on top of the pool of media to immobilize the wing discs. 50 µL of embryo oil was added along the outer periphery of the insert to seal. 100 µL of *organ culture* media was added on top of membrane of the insert. The setup was then transferred to a confocal microscope for Ca^{2+} activity imaging. Imaging was performed on a Nikon Eclipse T*i* confocal microscope (Nikon Instruments, Melville, NY) with a Yokogawa spinning disc and MicroPoint laser ablation system (Andor Technology, South Windsor, CT). Image data were collected on an iXonEM+ cooled CCD camera (Andor Technology, South Windsor, CT) using MetaMorph® v7.7.9 software (Molecular Devices, Sunnyvale, CA). All experiments were performed immediately following dissection to minimize time in culture, except for drug experiments that were incubated for one hour in drug solution or vehicle carrier control prior to imaging. Discs were imaged at a three z-planes with a step size of 10 µm, 20x magnification and 10-second intervals for a total period of one hour.

Data pre-processing

Microscopy resulted in 4D time-lapse data (512 pixels by 512 pixels by 3 z-planes by 361 time points). The z-stack data was max-projected in FIJI[46] to yield z-projected time-lapse videos. Discs that moved over the imaging session by more than several cell diameters were registered with the *StackReg* function in FIJI. Time points were selected such that discs were only analysed during times in which discs were immobile, with the shortest time-lapse analysed being 20 minutes (Extended Data Fig. 1).

For each disc, an ROI defining the pouch was manually selected in MATLAB, and a binary mask was generated. A Gaussian filter was applied to the mask to smooth the polygon into a disk shape. The major axis orientation was calculated for the mask, and the video was rotated such that the major axis was horizontal. The posterior (P) and dorsal (D) compartments were identified manually based on the characteristic shapes of the posterior and anterior compartments (Extended Data Fig. 3). Pouches were flipped such that the A compartment was on the left, and the D compartment was on the top.

Feature extraction

For each pouch sample, between 803 and 6,083 signals were obtained by taking average intensity (F(t)) from 4x4 pixel (2.8 µm x 2.8 µm) spatial bins arrayed with square packing across the segment disc pouch (Extended Data Fig. 1a). Video durations ranged from 20 to 60 minutes (Extended Data Fig. 1b-c). Each signal was decomposed into the following features: amplitude, frequency, duty cycle, and basal intensity, which comprise the Ca^{2+} signature of the ROI. Amplitude (Amp) is defined as the mean of the amplitudes of the peaks, where the amplitude of each peak is the prominence of the peak in the *findpeaks* algorithm. Frequency (F, mHz) is the number of peaks detected divided by the length of the signal in time. The duty cycle (D, % active / % inactive), is the percentage of time that the signal is “active”. This is measured as sum of the width at half max (WHM, s) of all peaks, divided by the total time of the signal, where WHM is defined as the time that a peak is above the peak value minus half the prominence. A

lower duty cycle represents a more rapid return to basal level. The basal intensity (B, arbitrary units) represents the equilibrium cytoplasmic concentration of Ca^{2+}, and is the minimum of the signal (Fig. 2, Extended Data Fig. d-e).

To reduce stochastic noise, the normalized intensity ($\Delta F(t)/F_o$) was approximated by using a bandpass Gaussian filter. Spikes in signalling activity were extracted from $\Delta F(t)/F_0$ using the MATLAB *findpeaks* algorithm, with a minimum amplitude (Amp_{min}), refractory period, and width at half max (WHM_{min}), for a total of five parameters. MATLAB's genetic algorithm *ga* was used to calibrate the feature extraction parameters (Fig. 2, Extended Data Fig. 3, Extended Data Table 4). To generate reference values, 233 signals (I(t)) were randomly selected from the 656,000 total signals, and manually annotated to identify the times (t_1 and t_2) at which each peak begins and ends. From this, the basal level was taken to be:

$$B_{manual} = \min\big(I(t\epsilon[t_1, t_2])\big)$$

the amplitude was extracted, as equal to:

$$Amp_{manual} = \max\big(I(t\epsilon[t_1, t_2])\big) - B_{manual}$$

and the width at half max (WHM) was taken to be:

$$\mathrm{WHM}_{manual} = \mathrm{sum}\left(I(t\epsilon[t_1, t_2]) > \frac{(Amp_{manual} - B_{manual})}{t_2 - t_1}\right)$$

The genetic algorithm was run at default settings for 172 generations. The objective function Err_1 was the sum of the squared differences of the correlation coefficients of the manual measurements and automatic measurements normalized to manual measurements. Err_2 was the fraction of signals with no waves incorrectly selected to contain waves compared to the manual ground-truth annotated data:

$$Err_1 = \sqrt{\left(\frac{Amp_{manual} - Amp_{auto}}{Amp_{manual}}\right)^2 + \left(\frac{WHM_{manual} - WHM_{auto}}{WHM_{manual}}\right)^2 + \left(\frac{B_{manual} - B_{auto}}{B_{manual}}\right)^2}$$

$$Err_2 = \frac{1}{N}\sum_{i}^{N}(WHM_{manual} = 0 \;\&\; WHM_{auto} > 0)$$

where N is the number of signals analysed (N = 233). A pareto front was generated to demonstrate the trade-offs between summary statistic error and false positives, and parameter values were selected (Extended Data Fig. 2, Extended Data Table 5).

Statistical Analysis

The median of ROIs in each disc for each summary statistics was compared across genetic conditions, pouch sizes, and between compartments (Fig. 2, Extended Data Fig. 3). ROIs within two spatial bins of the edge were excluded from the median, because several occasions would briefly drift out of frame. To compare across conditions, the two-tailed, unpaired, Student's t-test was performed. Significance was verified with the Wilcoxon rank sum test, which gave similar results (Extended Data Table 3). To compare across compartments, medians were taken after dividing discs into A compartment and P compartment such that the boundary was a vertical line fitted to points along the A/P axis as described in (Extended Data Fig. 3). The two-tailed, paired Student's t-test was performed. Significance was verified with the Wilcoxon signed-rank test,

which gave similar results. (Extended Data Table. 1). ANOVA was used to determine whether any size bin deviated from the group mean (Fig. 3). Violin plot composites were generated with the *distributionPlot* package from the empirical distributions of each disc, where 5,000 bootstrapped samples were obtained from each pouch or compartment to ensure that each biological sample contributed equally to the composite violin plot.

Visualization

To explore the impact of spatial position, developmental progression, and genetic/drug perturbations on Ca^{2+} signatures, we represented each disc as a spatial map, and obtained a spatial composite map for each condition. For each position x and y relative to the centroid of the disc, features were measured independently, and the median was displayed in the composite map (Fig 2-4, Extended Data Fig. 1). Median projections for each summary statistic were obtained. To convey the size of the average pouch in the composite, pixels containing fewer than half of the pouches in the sample were removed from the visualization.

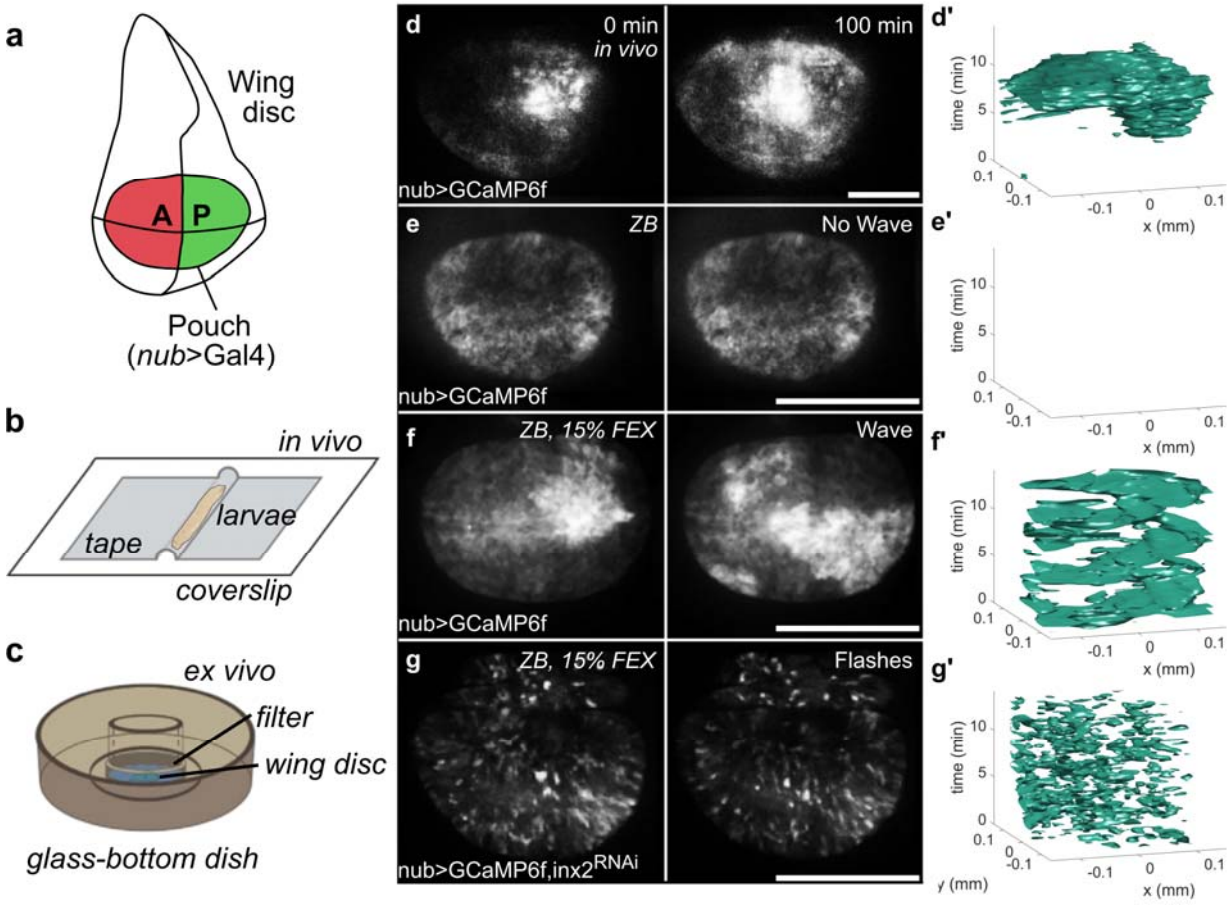

Figure 1 | Intercellular Ca^{2+} waves (ICWs) in *Drosophila* wing discs.
a, Cartoon of wing disc model system. The wing disc is subdivided into lineage-restricted anterior-posterior compartments. Gene expression in the pouch can be modulated with Gal4/UAS system using the *nubbin*-GAL4 driver. **b,** Wing disc imaged in the *in vivo* imaging setup. **c,** Wing disc *ex vivo* imaging setup. **d,** *In vivo* confocal imaging of GCaMP6f during an ICW **e-g,** *Ex vivo* confocal imaging of GCaMP6f. **e'-g',** Isosurface of GCaMP6f fluorescence over time: **e,** in ZB media; **f,** in ZB media with 15% FEX; **g,** wing discs with reduced gap junction communication through knockdown of *Inx2* in ZB media with 15% FEX.

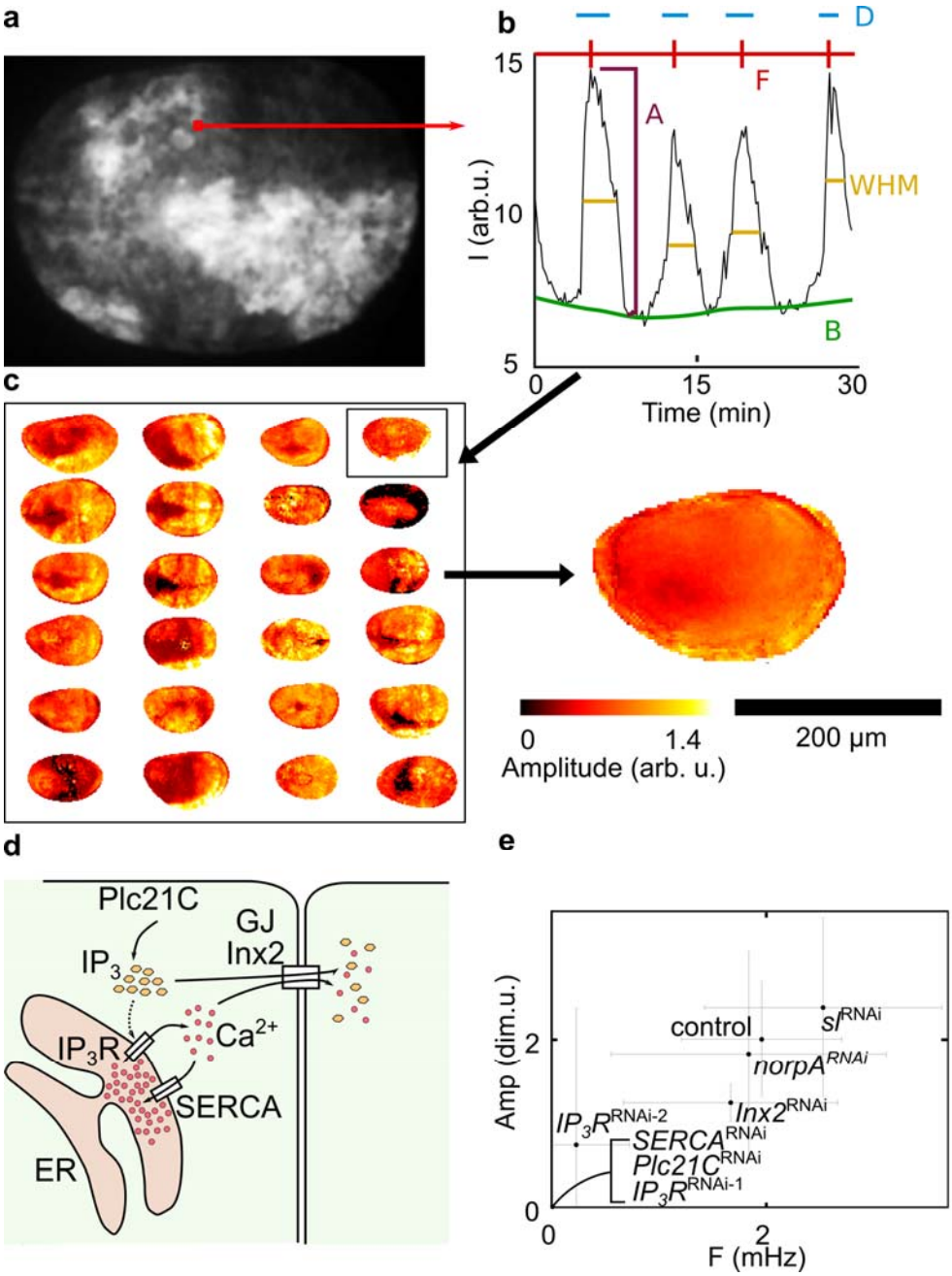

Figure 2 | ICWs are stimulated by FEX and requires Plc21C and IP_3R. a, Illustration of region-of-interest (ROI) based extraction of Ca^{2+} traces. **b,** Extraction of amplitudes (A), frequency (F), width at half max (WHM) and amplitude (A) from Ca^{2+} trace for individual regions-of-interest (ROI). Duty cycle (D) is WHM*F, which represents the average fraction of time that a cell is activated. **c,** Flowchart of generating composites. **d,** Schematic of ICW mechanism in the wing disc as verified by this study and previous work[6,11,28]. **e,** Average frequency and amplitude of ICWs in different genetic perturbation background. Error bars represent standard deviation. IP_3: inositol-1,4,5-trisphosphate; ER: endoplasmic reticulum; SERCA: sarco/endoplasmic reticulum Ca^{2+} ATPase; GJ: gap junction.

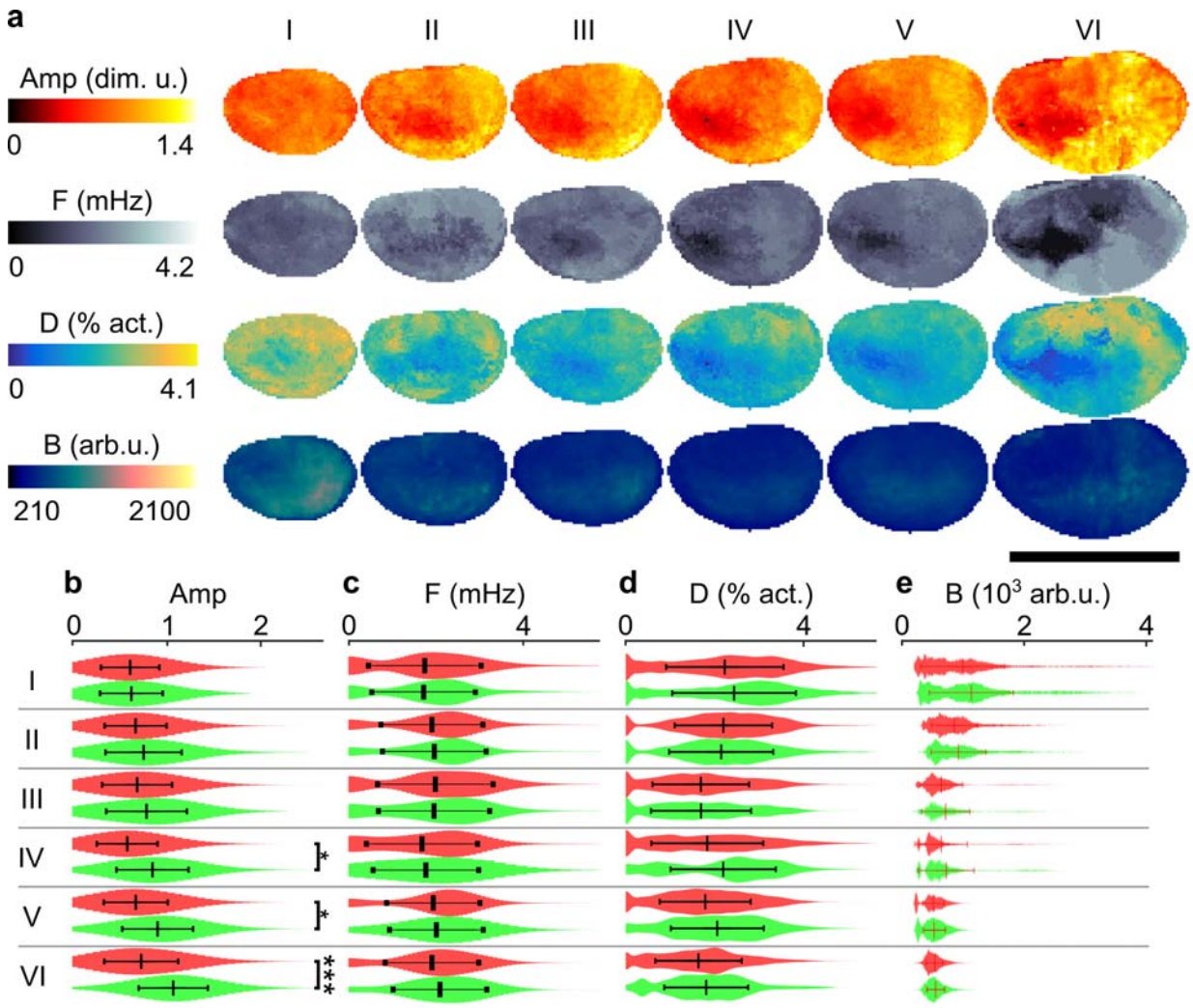

Figure 3 | ICWs are spatiotemporally patterned during development.
Composite maps of summary statistics extracted from *nub*-GAL4; UAS-GCaMP6f pouches binned by pouch size. Bins I (n=12 discs), II (n=8), III (n=17), IV (n=10), V (n=18), and VI (n=14) represent pouches with pouch areas of <14, 14-15.5, 15.5-17, 17-18.5, 18.5-20, and >20 x10^3 μm^2 respectively. M = 35 total imaging experiments. **a,** Composite spatial maps of the median ICW summary statistics. **b-e,** Distributions of individual bin values in A (red) and P (green) compartments for: **b,** amplitude, Amp (dim. u.), **c,** frequency, F (mHz), **d,** duty cycle, D (% active), **e,** and basal level, B (arb. u.). Scale bar represents 200 μm. * p<0.05, ** p<0.01, and *** p<0.001 by student t-test.

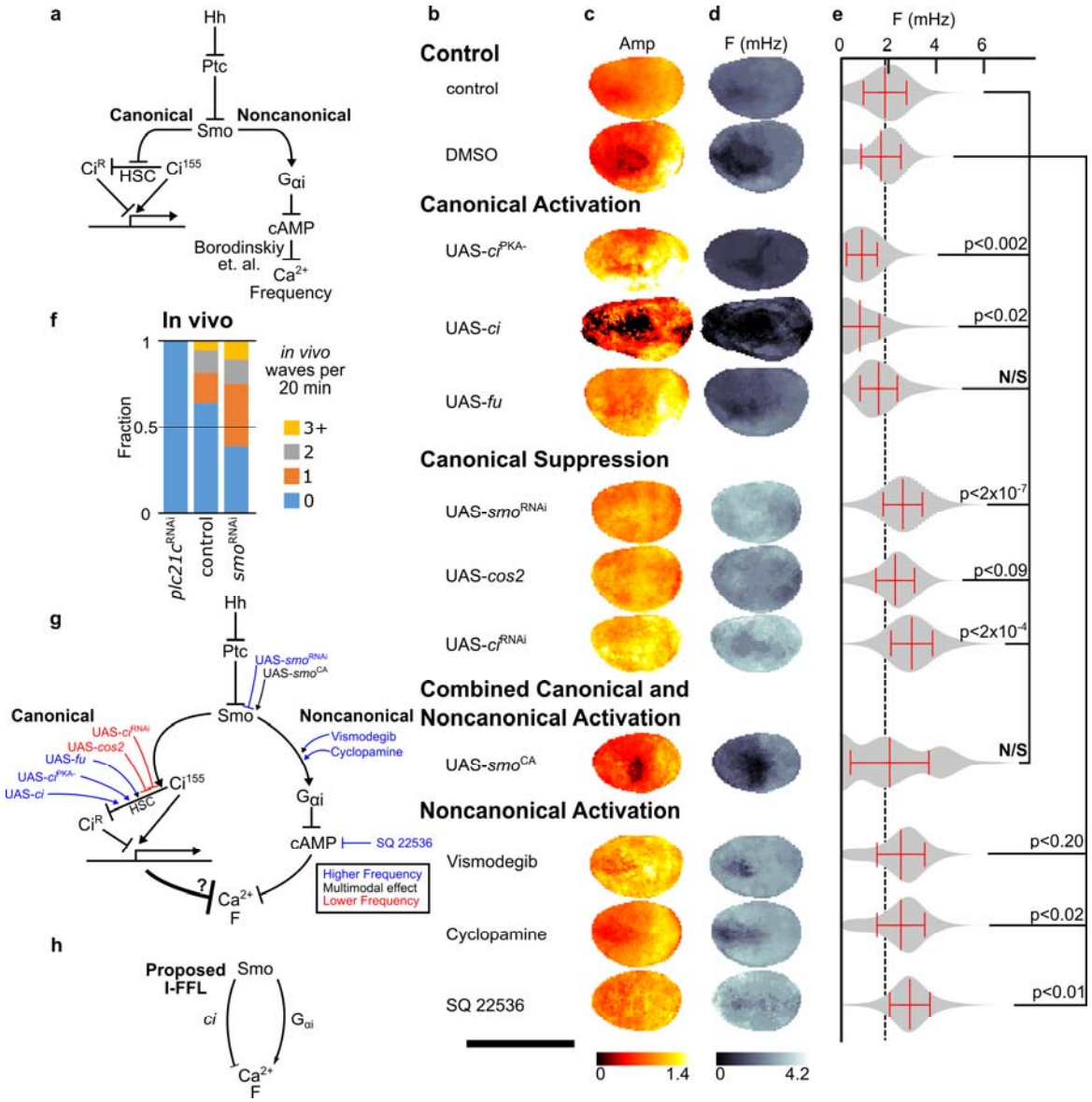

Figure 4 | Hedgehog signalling regulates ICW dynamics.

a, Schematic of Hh signalling pathway. **b,** Genetic or drug perturbation identity. **c-e,** Composite spatial maps of the median ICW summary statistics. Scale bar represents 200 μm. **c,** Amplitude, **d,** frequency, **e,** distribution of frequency values within discs, n = 76, 4, 18, 3, 14, 12, 10, 7, 14, 9, 19, and 7 discs. In e, red line error bars indicate average value with standard deviation. Genetic perturbations are compared to "control" (*nub*-GAL4; UAS-GCaMP6f), and pharmacological perturbations compared to "DMSO" (*nub*-GAL4; UAS-GCaMP6f treated with 0.1% DMSO for 1 hour). Dotted grey line indicates baseline frequency. P-values by Student's t-test. **f,** *In vivo* ICW frequency in immobilized larvae (n = 11, 72, and 28). *In vivo* results of ICWs match those of *ex vivo* results, where *Plc21c*^{RNAi} abolished ICWs and *smo*^{RNAi} increases ICW frequency. **g,** Proposed mechanism for regulation of ICW dynamics by Hh signalling. **h,** Proposed incoherent feed-ward loop (I-FFL). Scale bar: 200 μm.

References

1. Prevarskaya, N., Skryma, R. & Shuba, Y. Calcium in tumour metastasis: new roles for known actors. *Nat. Rev. Cancer* **11,** 609–618 (2011).
2. Markova, O. & Lenne, P.-F. Calcium signaling in developing embryos: focus on the regulation of cell shape changes and collective movements. *Semin. Cell Dev. Biol.* **23,** 298–307 (2012).
3. Monteith, G. R., Davis, F. M. & Roberts-Thomson, S. J. Calcium channels and pumps in cancer: changes and consequences. *J. Biol. Chem.* **287,** 31666–31673 (2012).
4. Antunes, M., Pereira, T., Cordeiro, J. V., Almeida, L. & Jacinto, A. Coordinated waves of actomyosin flow and apical cell constriction immediately after wounding. *J. Cell Biol.* **202,** 365–379 (2013).
5. Deng, H., Gerencser, A. A. & Jasper, H. Signal integration by Ca2+ regulates intestinal stem-cell activity. *Nature* **528,** 212–217 (2015).
6. Restrepo, S. & Basler, K. Drosophila wing imaginal discs respond to mechanical injury via slow InsP3R-mediated intercellular calcium waves. *Nat. Commun.* **7,** 12450 (2016).
7. Wallingford, J. B., Ewald, A. J., Harland, R. M. & Fraser, S. E. Calcium signaling during convergent extension in Xenopus. *Curr. Biol.* **11,** 652–661 (2001).
8. Berridge, M. J., Lipp, P. & Bootman, M. D. The versatility and universality of calcium signalling. *Nat. Rev. Mol. Cell Biol.* **1,** 11–21 (2000).
9. Clapham, D. E. Calcium Signaling. *Cell* **131,** 1047–1058 (2007).
10. Smedler, E. & Uhlén, P. Frequency decoding of calcium oscillations. *Biochim. Biophys. Acta BBA - Gen. Subj.* **1840,** 964–969 (2014).
11. Narciso, C. *et al.* Patterning of wound-induced intercellular Ca 2+ flashes in a developing epithelium. *Phys. Biol.* **12,** 056005 (2015).
12. Ohno, Y. & Otaki, J. M. Spontaneous long-range calcium waves in developing butterfly wings. *BMC Dev. Biol.* **15,** 1–13 (2015).
13. Chifflet, S. *et al.* Early and late calcium waves during wound healing in corneal endothelial cells. *Wound Repair Regen.* **20,** 28–37 (2012).
14. Justet, C., Hernández, J. A., Torriglia, A. & Chifflet, S. Fast calcium wave inhibits excessive apoptosis during epithelial wound healing. *Cell Tissue Res.* 1–14 (2016).
15. Antunes, M., Pereira, T., Cordeiro, J. V., Almeida, L. & Jacinto, A. Coordinated waves of actomyosin flow and apical cell constriction immediately after wounding. *J. Cell Biol.* **202,** 365–379 (2013).
16. Kuchibhotla, K. V., Lattarulo, C. R., Hyman, B. T. & Bacskai, B. J. Synchronous hyperactivity and intercellular calcium waves in astrocytes in Alzheimer mice. *Science* **323,** 1211–1215 (2009).
17. Davis, F. M. *et al.* Induction of epithelial–mesenchymal transition (EMT) in breast cancer cells is calcium signal dependent. *Oncogene* **33,** 2307–2316 (2014).
18. Turing, A. M. The Chemical Basis of Morphogenesis. *Philos. Trans. R. Soc. Lond. Ser. B* **237,** 37–72 (1952).
19. Ingham, P. W., Nakano, Y. & Seger, C. Mechanisms and functions of Hedgehog signalling across the metazoa. *Nat. Rev. Genet.* **12,** 393–406 (2011).
20. Tabata, T. & Kornberg, T. B. Hedgehog is a signaling protein with a key role in patterning Drosophila imaginal discs. *Cell* **76,** 89–102 (1994).
21. Robbins, D. J., Fei, D. L. & Riobo, N. A. The Hedgehog Signal Transduction Network. *Sci Signal* **5,** re6–re6 (2012).
22. Brennan, D., Chen, X., Cheng, L., Mahoney, M. & Riobo, N. A. Noncanonical Hedgehog Signaling. *Vitam. Horm.* **88,** 55–72 (2012).
23. Belgacem, Y. H. & Borodinsky, L. N. Sonic hedgehog signaling is decoded by calcium spike activity in the developing spinal cord. *Proc. Natl. Acad. Sci.* **108,** 4482–4487 (2011).

24. Sun, X. R. *et al.* Fast GCaMPs for improved tracking of neuronal activity. *Nat. Commun.* **4,** (2013).
25. Zartman, J., Restrepo, S. & Basler, K. A high-throughput template for optimizing Drosophila organ culture with response-surface methods. *Development* **140,** 667–674 (2013).
26. Burnette, M., Brito-Robinson, T., Li, J. & Zartman, J. An inverse small molecule screen to design a chemically defined medium supporting long-term growth of Drosophila cell lines. *Mol. Biosyst.* **10,** 2713–2723 (2014).
27. Handke, B., Szabad, J., Lidsky, P. V., Hafen, E. & Lehner, C. F. Towards Long Term Cultivation of Drosophila Wing Imaginal Discs In Vitro. *PLoS ONE* **9,** e107333 (2014).
28. Narciso, C. E., Contento, N. M., Storey, T. J., Hoelzle, D. J. & Zartman, J. J. A regulated environment for micro-organs defines essential conditions for intercellular Ca2+ waves. *bioRxiv* 081869 (2016). doi:10.1101/081869
29. Fraser, S. E. & Bryant, P. J. Patterns of dye coupling in the imaginal wing disk of Drosophila melanogaster. *Nature* **317,** 533–536 (1985).
30. Hufnagel, L., Teleman, A. A., Rouault, H., Cohen, S. M. & Shraiman, B. I. On the mechanism of wing size determination in fly development. *Proc. Natl. Acad. Sci.* **104,** 3835–3840 (2007).
31. Bessonov, N. *et al.* On a Model of Pattern Regeneration Based on Cell Memory. *PLOS ONE* **10,** e0118091 (2015).
32. Basler, K., Struhl, G. & others. Compartment boundaries and the control of Drosophila limb pattern by hedgehog protein. *Nat.-Lond.-* 208–208 (1994).
33. Dahmann, C., Oates, A. C. & Brand, M. Boundary formation and maintenance in tissue development. *Nat. Rev. Genet.* **12,** 43–55 (2011).
34. Rodriguez, I. & Basler, K. Control of compartmental affinity boundaries by Hedgehog. *Nature* **389,** 614–618 (1997).
35. Gibson, M. C. & Schubiger, G. Hedgehog is required for activation of engrailed during regeneration of fragmented Drosophila imaginal discs. *Development* **126,** 1591–1599 (1999).
36. Liu, C. *et al.* Hedgehog signaling downregulates Suppressor of Fused through the HIB/SPOP-Crn axis in Drosophila. *Cell Res.* **24,** 595–609 (2014).
37. Teperino, R. *et al.* Hedgehog Partial Agonism Drives Warburg-like Metabolism in Muscle and Brown Fat. *Cell* **151,** 414–426 (2012).
38. Alon, U. *An Introduction to Systems Biology: Design Principles of Biological Circuits*. (CRC Press, 2006).
39. Hart, Y., Antebi, Y. E., Mayo, A. E., Friedman, N. & Alon, U. Design principles of cell circuits with paradoxical components. *Proc. Natl. Acad. Sci.* **109,** 8346–8351 (2012).
40. Hart, Y. & Alon, U. The Utility of Paradoxical Components in Biological Circuits. *Mol. Cell* **49,** 213–221 (2013).
41. Gurdziel, K. *et al.* Identification and Validation of Novel Hedgehog-Responsive Enhancers Predicted by Computational Analysis of Ci/Gli Binding Site Density. *PLOS ONE* **10,** e0145225 (2015).
42. Alon, U. Network motifs: theory and experimental approaches. *Nat. Rev. Genet.* **8,** 450–461 (2007).
43. Yeger-Lotem, E. *et al.* Network motifs in integrated cellular networks of transcription–regulation and protein–protein interaction. *Proc. Natl. Acad. Sci. U. S. A.* **101,** 5934–5939 (2004).
44. Hart, Y. & Alon, U. The Utility of Paradoxical Components in Biological Circuits. *Mol. Cell* **49,** 213–221 (2013).
45. Bryant, P. J. & Fraser, S. E. Wound healing, cell communication, and DNA synthesis during imaginal disc regeneration in Drosophila. *Dev. Biol.* **127,** 197–208 (1988).

46. Schindelin, J. *et al.* Fiji: an open-source platform for biological-image analysis. *Nat. Methods* **9,** 676–682 (2012).